ACS APPLIED MATERIALS & INTERFACES

Research Article

www.acsami.org

Yeast Cells-Derived Hollow Core/Shell Heteroatom-Doped Carbon Microparticles for Sustainable Electrocatalysis

Xiaoxi Huang,[†] Xiaoxin Zou,[∥] Yuying Meng,[‡] Eliška Mikmeková,[#] Hui Chen,[∥] Damien Voiry,[§] Anandarup Goswami,[†,‡] Manish Chhowalla,[§] and Tewodros Asefa*[,†,‡,⊥]

[†]Department of Chemistry and Chemical Biology, Rutgers, The State University of New Jersey, Piscataway, New Jersey 08854, United States

[‡]Department of Chemical and Biochemical Engineering, Rutgers, The State University of New Jersey, Piscataway, New Jersey 08854, United States

[§]Department of Materials Science and Engineering, Rutgers, The State University of New Jersey, Piscataway, New Jersey 08854, United States

[⊥]Institute for Advanced Materials, Devices and Nanotechnology (IAMDN), Rutgers, The State University of New Jersey, Piscataway, New Jersey 08854, United States

[∥]State Key Laboratory of Inorganic Synthesis & Preparative Chemistry, College of Chemistry, Jilin University, Changchun 130012, China

[#]Institute of Scientific Instruments of the ASCR, Brno 612 64, Czech Republic

Supporting Information

ABSTRACT: The use of renewable resources to make various synthetic materials is increasing in order to meet some of our sustainability challenges. Yeast is one of the most common household ingredients, which is cheap and easy to reproduce. Herein we report that yeast cells can be thermally transformed into hollow, core−shell heteroatom-doped carbon microparticles that can effectively electrocatalyze the oxygen reduction and hydrazine oxidation reactions, reactions that are highly pertinent to fuel cells or renewable energy applications. We also show that yeast cell walls, which can easily be separated from the cells, can produce carbon materials with electrocatalytic activity for both reactions, albeit with lower activity compared with the ones obtained from intact yeast cells. The results reveal that the intracellular components of the yeast cells such as proteins, phospholipids, DNAs and RNAs are indirectly responsible for the latter's higher electrocatalytic activity, by providing it with more heteroatom dopants. The synthetic method we report here can serve as a general route for the synthesis of (electro)catalysts using microorganisms as raw materials.

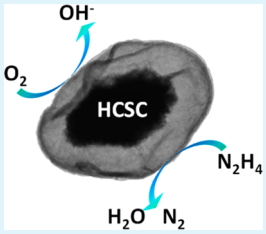

KEYWORDS: *yeast, heteroatom-doped carbon, oxygen reduction, ORR, hydrazine electrooxidation*

INTRODUCTION

Over the past three decades, carbon nanomaterials have captured scientists' imagination because of their fascinating properties as well as numerous potential applications. The past few years are no exception; amidst the strings of their known unique properties, the recent reports on carbon nanomaterials' interesting catalytic properties for a number of important reactions,[1,2] e.g., the hydrogen evolution reaction (HER),[3] the oxygen evolution reaction (OER)[4,5] and the oxygen reduction reaction (ORR),[6−11] have been equally captivating. Moreover, because the materials can be synthesized from a variety of carbon precursors, both synthetic as well as natural ones, the materials have also been fascinating from a synthetic point of view. Although many synthetic substances such as dicyandiamide,[3] polyaniline,[11] phenol and triphenylphosphine,[7] polypyrrole,[12,13] etc. have been successfully employed as precursors for making carbon materials with good electrocatalytic activity, most of them are toxic and unfriendly to the environment. Hence, natural precursors, especially those that are relatively cheap, abundant, renewable and environmental friendly, are preferred, and can constitute sustainable synthetic routes for these catalysts. Such precursors can generally be divided into two groups: (1) inanimate sources such as cellulose,[14] silk cocoon,[15] corn protein,[16] hemoglobin,[17] and human urine[18] and (2) living organisms such as microalgae,[19] grass,[20] plant *Typha orientalis*,[21] peat moss,[22] etc. More importantly, as many of these precursors inherently contain nitrogen and other heteroatoms, they can directly lead to heteroatom-doped carbon materials by simple pyrolysis. This is quite important because the heteroatom species present on carbon nanomaterials are the ones mainly responsible for the materials' electrocatalytic activity toward reactions such as ORR[20,23,24] and hydrazine oxidation reaction (HOR).[12,14,25] Moreover, because through powerful techniques of genetic engineering

Received: November 7, 2014
Accepted: December 30, 2014
Published: December 30, 2014

DOI: 10.1021/am507787t
ACS Appl. Mater. Interfaces 2015, 7, 1978−1986

Scheme 1. Schematic Illustration of Procedures Used for Making Heteroatom-Doped Hollow, Core/Shell Carbon and Yeast Cell Wall Carbon from Yeast Cell and Yeast Cell Wall, Respectively[a]

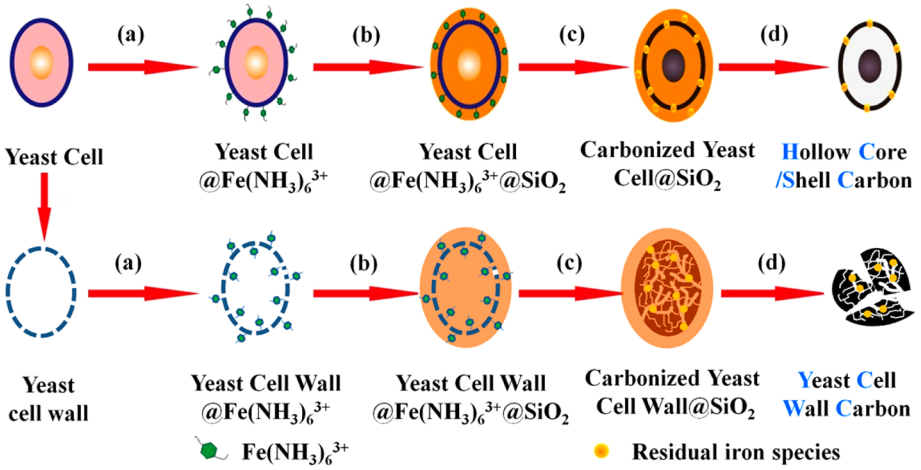

[a](a) Adsorption of $[Fe(NH_3)_6]^{3+}$ ions around yeast cells and yeast cell wall particles, (b) deposition of silica shells, (c) high temperature treatment of the yeast/metal ions/silica, and (d) removal of the silica shells.

and biotechnology, mutations and insertion of unnatural amino acid into the structure of natural raw materials can easily be done,[26] such biological precursors could have the potential to form carbon-based materials with precisely controlled dopant density and interesting, tunable properties.

Yeasts, which are members of fungi, can serve as ideal, natural precursors from which to make carbon electrocatalysts. Their subcellular structure (cell walls, membranes, nuclei, organelles), which are similar to those of higher animal and plant cells,[27] can all easily be transformed to carbon materials by pyrolysis. Moreover, yeasts are easy to culture or grow in large quantity, are nontoxic and have reasonably uniform morphology. Thus, it is not surprising that yeast cells have received some attention from materials researchers for their potential application as templates to make various hollow metal oxides, e.g., hollow silica microspheres.[28] Recently, yeast has also been demonstrated to serve as template for $CoFe_2O_4$ and then give $CoFe_2O_4$/amorphous biocarbon composite material for electrocatalysis.[29]

Herein we show that the baker's yeast cells (*Saccharomyces cerevisiae*) can be used as a precursor to make hollow, core/shell type heteroatom-doped carbon microparticles (denoted as HCSC hereafter) that can electrocatalyze ORR and HOR (Scheme 1). We also show that yeast cell wall particles extracted from yeast (YCWPs),[30] which are hollow, porous 2−4 μm particles containing β-1,3-D-glucan, chitin and some mannoproteins, can lead to carbon microparticles (labeled as yeast cell wall-derived carbons or YCWC). The resulting material can catalyze ORR and HOR, albeit with less activity than HCSC. It is worth noting here that both types of materials we synthesized here have different compositions, structures, as well as properties, and also involve different synthetic routes compared with the few other materials reported previously using yeast as templates, as mentioned above.[28,29]

EXPERIMENTAL SECTION

Materials and Reagents. Tetraethyl orthosilicate (TEOS), iron(III) chloride ($FeCl_3$), potassium hydroxide (KOH), hydrazine, Nafion and ammonia solution (30%) were purchased from Sigma-Aldrich. Sodium hydroxide (NaOH), hydrochloric acid and absolute ethanol were obtained from Fisher Scientific. All the reagents were of analytical grade and used as received without further purification. Deionized water was used throughout the experiments.

Synthesis of Hollow Core−Shell Carbon (HCSC) Electrocatalyst from Yeast Cells. To a dispersion of yeast cells (4 g) in a solution of water/ethanol (60 mL/120 mL) was added $FeCl_3$ (0.1 mmol). After the dispersion was stirred for 30 min, ammonia solution (4.2 mL, 30%) was added into the dispersion. After the dispersion was stirred for another 30 min, TEOS (5 mL) was added into it. The solution was then sonicated in an ultrasonic bath for 1 h and stirred for another 18 h. The precipitate was recovered by centrifugation and washed with ethanol (25 mL) three times (via sonication, centrifugation and decantation). Then, 400 mg of the resulting material was placed in a temperature-programmable tube furnace and was heated in a N_2 atmosphere from room temperature to 200 °C at 1 °C/min. The furnace temperature was kept at 200 °C for 2 h. The temperature was subsequently increased to 300 °C at 1 °C/min and kept at this temperature for 2 h. Finally, the furnace temperature was raised to 900 °C at a ramp of 10 °C/min and kept at 900 °C for 2 h. The furnace was then let to cool down to room temperature at a ramp of 10 °C/min. The silica shells from the resulting silica-coated carbon nanomaterial were etched by stirring the material in 16 mL 1.25 M NaOH solution in an autoclave for 18 h at 100 °C. A black powdered material was recovered via centrifugation of the dispersion. The solid material was then sonicated with water, and the dispersion was filtered. The solid product was washed with water until the supernatant becomes neutral, ensuring the complete removal of residual base off the solid material. This finally afforded the HCSC material.

Synthesis of Hollow Yeast Cell Wall Particles (YCWPs). YCWPs were prepared following the previously reported procedures.[30] A suspension of yeast (50 g) in 500 mL of 1 M NaOH solution was prepared, and the suspension was heated at 80 °C for 1 h. The solid material containing the yeast cell walls was collected by centrifugation and then suspended in 500 mL of deionized water. After the pH of the solution was adjusted to 4−5 by using 2 M HCl solution, the solution was incubated at 55 °C for 1 h. The insoluble residue was collected by centrifugation and washed with 500 mL deionized water, then with 100 mL of isopropyl alcohol four times, and finally with 100 mL of acetone twice. After letting the solid product dry at ambient conditions, a fine powdered material composed of yeast cell wall particles (denoted here as YCWPs), with a yield of ca. 12.5%, was obtained.

Synthesis of Electrocatalysts from YCWP. Into a dispersion of YCWP (500 mg) in a solution of water/ethanol (60 mL/120 mL) was added $FeCl_3$ (0.1 mmol). The dispersion was stirred for 30 min, after which ammonia solution (4.2 mL, 30%) was added into it. After the

DOI: 10.1021/am507787t
ACS Appl. Mater. Interfaces 2015, 7, 1978−1986

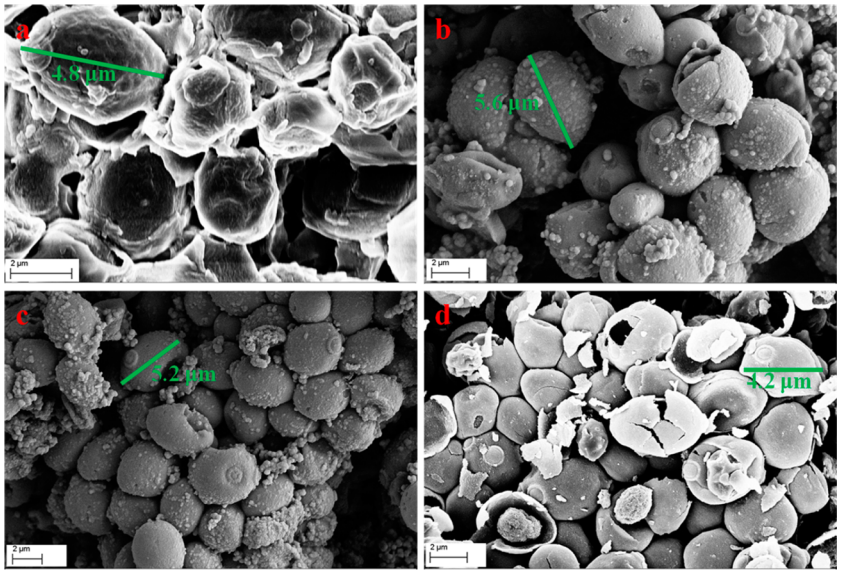

Figure 1. FESEM images of (a) yeast cells, (b) yeast cell@$[Fe(NH_3)_6]^{3+}$@SiO_2 microparticles, (c) carbonized yeast cell@SiO_2 microparticles and (d) hollow core/shell carbon (HCSC) microparticles.

dispersion was stirred for another 30 min, TEOS (5 mL) was added into it. The dispersion was then sonicated in an ultrasonic bath for 1 h and then stirred over magnetic stir plates for 18 h. The precipitate was recovered by centrifugation and washed with ethanol (25 mL) three times (via sonication, centrifugation and decantation). Then, 400 mg of the resulting material was pyrolyzed under exactly the same way as the procedure used for yeast cells above. The silica shells from the resulting material were etched by stirring the latter in 16 mL 1.25 M NaOH solution in autoclave for 18 h at 100 °C. A black powdered product was obtained after centrifugation of the dispersion. After washing the solid product with water until the supernatant is neutral (indicating complete removal of residual base off the material), YCWP-derived carbon microparticles, denoted as YCWCs, were obtained.

Electrocatalytic Oxygen Reduction Reaction (ORR) and Preparation of Working Electrodes for ORR. The electrocatalytic activities of the materials toward the oxygen reduction reaction (ORR) were investigated with a three-electrode cell using a Pine bipotentiostat (Pine Research Instrumentation). The cell consisted of a saturated calomel electrode (SCE) as the reference electrode, a carbon rod (diameter: 6 mm) as a counter electrode, and a glassy carbon disk (diameter: 5 mm) (GCE) with the catalysts as a working electrode, respectively. To prepare the working electrode, 2 mg of the sample was first dispersed in 200 μL of 2-propanol under sonication to get a homogeneous mixture, and 4 μL of this suspension was then drop-casted onto the surface of a freshly polished GCE. The final catalyst loading was 203 $\mu g/cm^2$. After letting the catalyst-coated electrode surface dry under ambient conditions, a solution of Nafion (4 μL) was drop-casted on the top of the electrode and allowed to dry completely. Cyclic voltammetry analyses were performed at a scan rate of 100 mV/s in O_2-saturated and N_2-saturated 0.1 M KOH solutions. The linear sweep voltammograms (LSVs) were obtained on a rotating ring-disk electrode (RDE) at a scan rate of 10 mV/s in oxygen saturated 0.1 M KOH solution at different rotating speeds, ranging from 400 to 2000 rpm.

The overall electron transfer number (n) for electrochemical oxygen reduction were obtained from the slopes of Koutechy–Levich plots using the following equation (eq 1):[13]

$$1/J = 1/J_L + 1/J_K = 1/(B\omega^{1/2}) + 1/J_K \quad (1)$$

where J, J_L and J_K are the measured current density, diffusion-limiting current density and kinetic current density, respectively, and ω is the electrode's rotation speed. The kinetic current is obtained from the intercept of Koutechy–Levich plots. The value of B can be calculated from the following equation (eq 2):

$$B = 0.62nFv^{-1/6}CD^{2/3} \quad (2)$$

where n is the electron transfer number, F is the Faraday constant (96 500 C/mol), v is the viscosity of the electrolyte solution (v = 0.01 cm^2/s), C is the concentration of O_2 in the electrolyte ($C = 1.2 \times 10^{-6}$ mol/cm^3) and D is the oxygen diffusion coefficient ($D = 1.9 \times 10^{-5}$ cm^3/s).

The number of electrons transferred (n) was also determined from RDE-based electrochemical results with an alternative method, using eq 3:

$$n = 4 \times J_D/(J_D + J_R/N) \quad (3)$$

where J_D is the disk current, J_R is the ring current, and N is the collection efficiency.

The percentage of hydrogen peroxide in the products (% H_2O_2) was calculated based on the equation below (eq 4):

$$\%H_2O_2 = 200 \times J_R/(J_D \times N + J_R) \quad (4)$$

Electrocatalytic Hydrazine Oxidation Reaction (HOR) and Preparation of the Working Electrodes for HOR. The eletrocatalytic properties of HCSC and YCWC synthesized above for HOR were evaluated with a PAR (Princeton Applied Research) Versastat3 potentiostat using a three-electrode configuration. The cell consisted of SCE as the reference electrode, a carbon rod (diameter: 6 mm) as the counter electrode and a GCE (diameter: 3 mm) with catalyst as the working electrode. To prepare the working electrode, 2 mg of the sample was first dispersed in 200 μL of 2-propanol via sonication to form the catalyst suspension, and 2 μL of this suspension was then drop-casted onto the surface of a freshly polished GCE. The final catalyst loading was 283 $\mu g/cm^2$. After the catalyst-coated electrode surface was let to dry under ambient conditions, a solution of Nafion (2 μL) was drop-casted on the top of the electrode and allowed to dry completely. Cyclic voltammetry (CV) and electrocatalysis were conducted in phosphate buffered saline (PBS) solution at pH = 7.4. In the cyclic voltammetry measurements, the electrode potential was scanned from −0.6 to +0.6 V vs SCE at 10 mV/s, in various concentrations of hydrazine (0, 6.4, 12.8, 19.2, 25.6, 32 and 64 mM). All the electrochemical measurements were performed at room temperature and under ambient pressure.

Characterizations. X-ray diffraction patterns of the materials were recorded on Rigaku D/Max 2550 X-ray diffractometer operating with the wavelength λ = 0.154 05 nm of Cu Kα radiation. The pore

DOI: 10.1021/am507787t
ACS Appl. Mater. Interfaces 2015, 7, 1978−1986

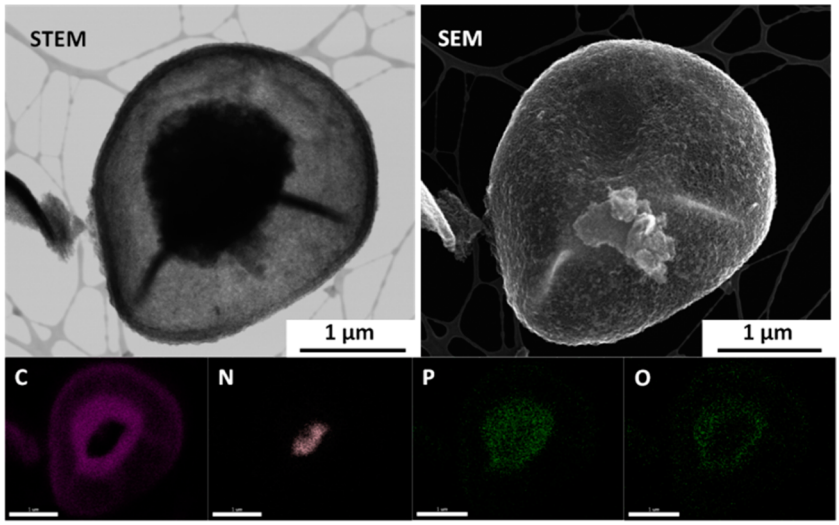

Figure 2. STEM and SEM images of HCSC and elemental mapping results for C, N, P and O atoms in them. The scale bars in all the images represent 1 μm.

properties of all the samples were investigated by physical adsorption of nitrogen at the liquid-nitrogen temperature (−196 °C) using a Micromeritics TriStar-3000 (Micromeritics Instrument Corp., USA). Before each measurement, the samples were first degassed for 6 h at 70 °C. The Brunauer−Emmett−Teller (BET) surface area and Barrett−Joyner−Halenda (BJH) pore size distribution of the samples were determined from the adsorption/desorption data. The Raman spectra were obtained using a Renishaw Raman spectrometer, model 1000, operating with a 20 mW air-cooled argon ion laser (λ = 514.5 nm) as the excitation lights source. The laser power at the sample position was typically 400 μW with an average spot-size of 1 μm in diameter. Elemental composition of the materials was probed with X-ray photoelectron spectroscopy (XPS) using a ESCALAB 250 X-ray photoelectron spectrometer equipped with an A1 Kα radiation as a source (hυ = 1486.6 eV), with an energy resolution of 1 eV for the survey scan and 0.1 eV for high resolution scans of the individual peaks. Field emission scanning electron microscopy (FESEM) images were taken with a Zeiss Sigma field emission SEM. Other microscope results were obtained from XHR S(T)EM Magellan 400 (FEI), which is equipped with EDS system for elemental analyses in the sample. The samples were further characterized by state-of-the-art scanning low energy electron microscopy (SLEEM, SEM equipped with a cathode lens system, CL) and low voltage scanning transmission electron microscopy (LV STEM). HAADF images were then acquired by collecting high-angle scattered electrons, whose contrast is strongly dependent on the average atomic number of the scatterer encountered by the incident probe.

RESULTS AND DISCUSSION

The synthetic process employed to make HCSC is illustrated in Scheme 1, and also discussed in more detail in the Experimental Section. First, an ammoniacal solution of Fe(III) ions was mixed with yeast cells. The solution was then stirred to allow adsorption of Fe(III) ions onto the cells. Using the sol−gel method, the yeast cells were subsequently coated with silica shells, aided by the Fe(III) ions present on the yeast cells' surfaces that allowed adsorption of the negatively charged silicate species formed in the solution. After this step, the size of the particles increased and their surfaces became smoother, indicating the deposition of silica shells around the yeast cells or the formation of cell@$Fe(NH_3)_6^{3+}$@SiO_2 microparticles (Figure 1a,b). Pyrolysis of the resulting cell@$Fe(NH_3)_6^{3+}$@SiO_2 microparticles was carried out, first at lower temperatures (first at 200 °C for 2 h and then at 300 °C for 2 h). This allowed the yeast cells to undergo carbonization without compromising their overall structure. The carbonized material was subsequently treated at a much higher temperature (900 °C) for 2 h, which made the carbon to undergo graphitization, assisted by the Fe(III) ions present in the material.[14,31] The FESEM images of the resulting material (Figure 1c) show that the morphology of silica shells remains intact even after such high temperature treatment. The result also indicates that the silica shells on the outer surfaces of the yeast cells let the yeast cells remain isolated during pyrolysis and keep their carbon species (some of which are possibly volatile) to reside inside the cores of the material. Finally, the silica shells were removed by dissolution with aqueous NaOH solution, resulting in hollow core/shell carbon or HCSC (Figure 1d).

The YCWC was prepared using YCWP as a precursor under an otherwise identical procedure. Also, for comparative studies, two more control materials were prepared by pyrolysis of the yeast cells or YCWPs without protecting their surfaces with silica shells (see more details in the Supporting Information). Unlike the hollow structures observed in HCSC, no hollow core/shell structure is seen in the case of YCWC (Figure S1d, Supporting Information). Moreover, the two control materials without silica shells show very large, bulky carbon structures (Figure S2, Supporting Information); this means, in the absence of silica shells, the yeast cells subjected to carbonization randomly deposit, grow uncontrollably and lead to chunky shaped, large-sized carbon particles. So, these results successfully demonstrate the importance of cells functionalized with silica for making highly porous carbon nanomaterials through pyrolysis, and how these properties are useful for the potential applications of the resulting materials for electrocatalysis (vide infra). It is worth noting that researchers have previously shown that living cells functionalized with polymers and inorganic nanoparticles can lead to various materials with many potential applications.[32] For example, polyelectrolyte-mediated assembly of multiwall carbon nanotubes on yeast cells has been shown to have potential application for microelectronic devices.[33] In another example, the potential applications of biotin-functionalized SiO_2-coated yeast cells immobilized onto avidin-modified surfaces cell-based for sensors were described.[34]

DOI: 10.1021/am507787t
ACS Appl. Mater. Interfaces 2015, 7, 1978−1986

The STEM and SEM images (Figure 2) of HCSC clearly show that this material contains elliptical-shaped, hollow core/shell carbon microparticles. In other words, HCSC appears to retain the original shapes of the yeast cells, where the cell walls transform into shells while the nuclei of the cells become cores, during which the cell membranes as well as the cytoplasm provide additional carbon atoms and heteroatom dopants to the resulting carbon structures. The resulting HCSC particles have taken the inherently elliptical morphology of yeast cells; this result is consistent with a previous report where hollow capsules templated by yeast cells were shown to retain the original elliptical shape of yeast cells after template removal.[35] Elemental mapping shows that HCSC is composed mainly of C, N, P and O atoms, with the elemental distribution of each particle varying from the shell to the center of each particle (Figure 2). Generally, more N, P and O dopant atoms are found in the cores than in the shells of HCSC, as seen from the elemental analyses results compiled in Table S1 (Supporting Information). This is most likely due to the presence of higher amounts of DNA, RNA and proteins in the nuclei of yeast cells. So, our results additionally suggest that yeast is a unique precursor in terms of producing carbon microparticles, with unusual elemental composition or compositional gradient on a nanoscale, or carbon nanomaterials that are hard to come by with other chemical synthetic methods, to the best of our knowledge.

The pore structures of HCSC and YCWC were investigated by nitrogen adsorption/desorption analyses, the results of which are summarized in Table 1. The isotherms show hysteresis loops (Figure S4a, Supporting Information), indicating the presence of mesoporous structure in both materials. Although the results reveal that the specific BET surface area of HCSC (250 m^2 g^{-1}) is lower than that of YCWC (912 m^2 g^{-1}), it is still much higher than that of the yeast-derived $CoFe_2O_4$/amorphous biocarbon material recently reported, whose value is only 79.8 m^2 g^{-1}.[29] The BJH pore volume and pore size (Figure S4b, Supporting Information) of HCSC (0.37 cm^3 g^{-1} and 10.7 nm, respectively) are higher than those of YCWC (0.29 cm^3 g^{-1} and 2.6 nm, respectively). It should be noted that the very large space between the shell and core of HCSC is not included in this pore volume analysis because it is out of the range of typical N_2 gas adsorption measurements. As can be seen from the digital images of YCWC and HCSC (Figure S4c, Supporting Information), the volume occupied by a given mass of HCSC is still much larger than that of YCWC. This is most likely due to the fact that there is no material in the center of YCWP to support the carbon structure forming from it, subsequently making the YCWC to collapse. In contrast, the hollow structures in HCSC remain intact due to the presence of some materials inside the cores of its precursor, as also seen in its corresponding microscopy images.

Table 1. BET Surface Area and BJH Pore Volume, Pore Size Summary for Different Samples

	BET surface area (m^2 g^{-1})	BJH pore volume (cm^3 g^{-1})	Average BJH pore size (nm)
YCWC	912	0.29	2.6
HCSC	250	0.37	10.7
yeast cell wall-derived carbon (without using silica shells)	7.5		
yeast cell-derived carbon (without using silica shells)	0.2		

The control carbon materials, prepared via pyrolysis of yeast cell wall or yeast cell without using silica shell for protection, are also studied with nitrogen adsorption/desorption measurements. Their BET surface areas are found to be very small, with the former giving only 7.5 m^2 g^{-1} and the latter giving 0.2 m^2 g^{-1}. This result is consistent with those obtained with SEM above. The results also once again indicate the importance of the silica shells in the synthesis of yeast-derived carbon materials with high surface areas. In other words, in the absence of silica shells around them, the yeast cells or cell walls undergo decomposition during pyrolysis and grow uncontrollably into bulk carbon materials with smaller surface areas.

The X-ray diffraction (XRD) patterns (Figure 3a) of HCSC and YCWC show broad peaks at *ca.* 2θ = 24° (002) and 44° (100). The (100) reflection is typically due to crystalline structure formed by sp^2 hybridized carbons, whereas the (002) reflections is associated with coherent and parallel stacking of graphene-like sheets.[18] The broad peaks indicate that the material is composed predominantly of amorphous or disordered carbon.

The elemental compositions of the materials, determined by X-ray photoemission spectroscopy (XPS) (Figure S5, Supporting Information) suggest that HCSC and YCWC are composed mainly of C, O, N, P and Fe. Additional XPS results depicted in Figure 3b shows that HCSC contains more heteroatom dopants than YCWC. This is most likely because the inner part (nucleus and organelles) of the yeast cells contains more heteroatoms, which can ultimately end up as dopants in the carbon materials (or HCSC, in this case). High resolution XPS spectra of P 2p electrons in both HCSC (Figure S5c, Supporting Information) and YCWC (Figure S 5d, Supporting Information) show a peak at around 132.8 eV, which can be attributed to P═O/P—O moieties. This is not totally unexpected because phosphorus atoms are generally bonded with oxygen atoms in many biological systems, including yeast cells, and they can thus easily end up as P═O/P—O species after pyrolysis of the silica-coated yeast cells or YCWPs. The high resolution N 1s spectra are deconvoluted into four peaks at 398.7, 400.3, 401.2 and 403.3 eV that correspond to pyridinic-N, pyrrolic-N, quaternary-N and pyridinic-N^+-O^- species. The ratios of all these different types of nitrogen species versus carbon are higher for HCSC compared with those of YCWC (Figure 3c). Based on the high-resolution C 1s spectra (Figure S5h, Supporting Information), more unsaturated oxidative carbon species (C═O at 287.5 eV, C═O—OH at 289.2 eV and benzylic species with $\pi-\pi^*$ satellite peak at 290.6 eV) are present in YCWC than in HCSC (Figure S5g, Supporting Information). This difference is ascribed to the large amount of protein and nucleic acid present in the intact yeast cells and their ability to serve as reducing agent, leading to less oxidized form of carbon (as HCSC). The amount of Fe determined by analyzing the Fe 2p peak on XPS is 0.25% for HCSC but undetectable for YCWC.

In addition, inductively coupled plasma optical emission spectrometry (ICP-OES) was used to measure the total amount of Fe in HCSC and YCWC. The results indicated that the weight percentages of Fe in HCSC and YCWC are 0.048% and 0.11%, respectively. When these results are combined with those obtained from XPS (which showed the presence of Fe species in HCSC but not so in YCWC), it can be concluded that the majority of Fe is present on the surfaces

DOI: 10.1021/am507787t
ACS Appl. Mater. Interfaces 2015, 7, 1978−1986

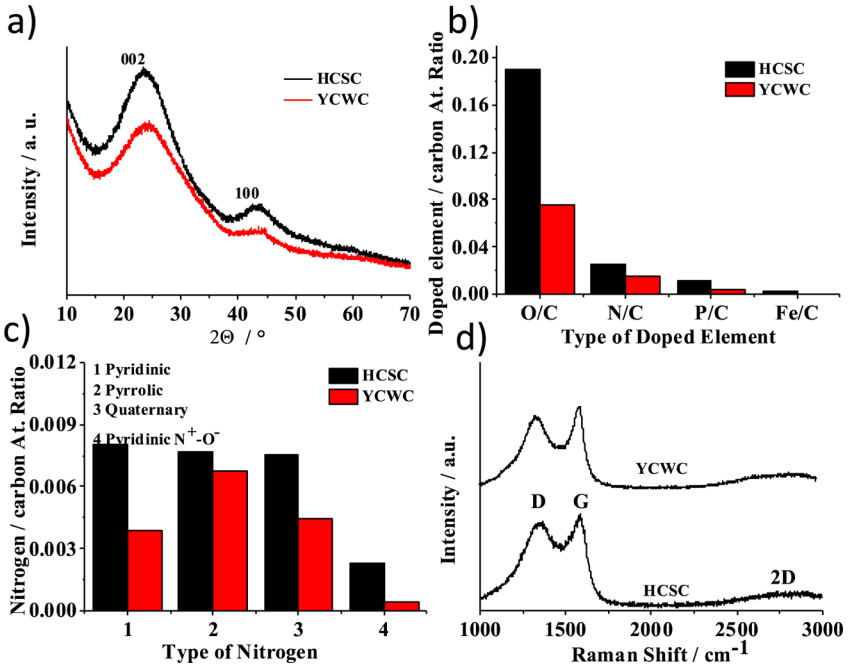

Figure 3. (a) XRD patterns of HCSC and YCWC. (b) Comparison of the ratios of atomic percent of dopant atoms to that carbon, or (O, N, P or Fe)/C for HCSC versus YCWC. (c) Comparison of the ratios of different types of N species/C atoms for HCSC versus YCWC. (d) Raman spectra of HCSC and YCWC.

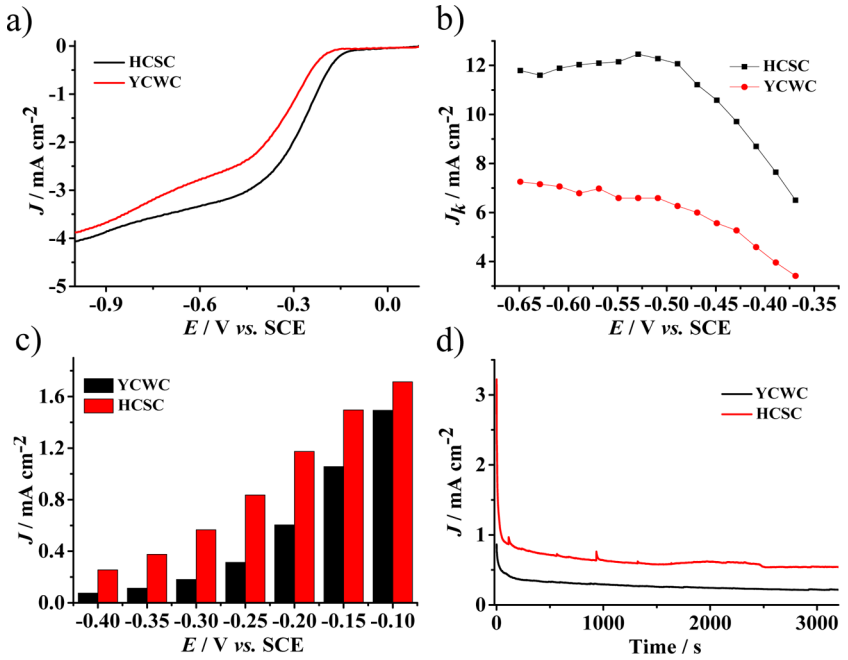

Figure 4. (a) Polarization curves of ORR at 1600 rpm on HCSC and YCWC. (b) Comparison of kinetic current density (J_k) of ORR at various potentials on HCSC and YCWC. (c) Comparison of current density of HOR at various potentials on HCSC and YCWC in 32 mM hydrazine. (d) Chronoamperometric results of electrocatalytic HOR of 50 mM hydrazine at −0.15 V over HCSC and YCWC.

in the case of HCSC but not so in the case of YCWC. Conversely, the results suggest that the Fe species that were combined with the intact yeast cell did not penetrate much into the center of the cells, or not as much as they did in the YCWC. On the other hand, the more permeable property of the YCWPs allowed the Fe species to diffuse into the inner part of the hollow particles and get encapsulated by the final porous carbon structure forming around them during pyrolysis, as illustrated in Scheme 1. The low amount of Fe in both materials is most likely because the Fe atoms are also etched when the pyrolyzed carbon/silica composite materials are treated in basic solution to remove the silica shells.[14] More importantly though, based on the above results as a whole, HCSC has more surface Fe atoms, besides other heteroatom dopants in its structure, than YCWC.

The Raman spectra (Figure 3d) of HCSC and YCWC reveal two broad peaks centered at ca. 1000 and 1700 cm^{-1}, and a less intense peak centered at ca. 2700 cm^{-1}, which can be attributed

DOI: 10.1021/am507787t
ACS Appl. Mater. Interfaces 2015, 7, 1978−1986

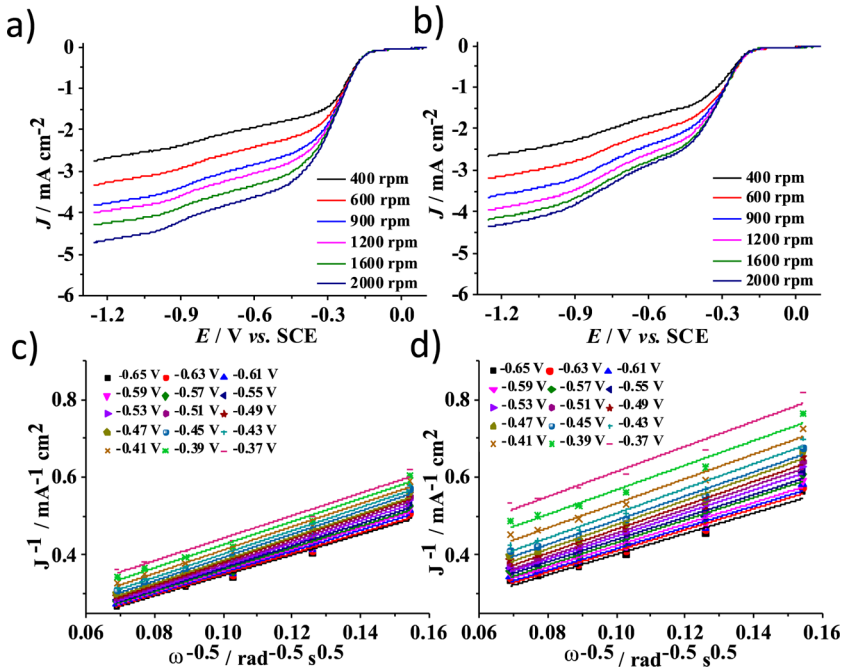

Figure 5. RDE polarization curves for (a) HCSC and (b) YCWC in O_2-saturated 0.1 M KOH solution at different RDE rotating speeds, and the corresponding Koutechy–Levich (K-L) plots derived from linear sweep voltammetry (LSV) results at different potentials for (c) HCSC and (d) YCWC.

to the D, G and 2D, respectively, of graphitic carbons. While the G band reveals the presence of graphitic structure in the carbon materials, the D band is generally related with structural defects, which in this case is due to the presence of heteroatom dopants in the porous carbon materials. The I_D/I_G ratios for HCSC and YCWC are 0.94 and 0.90, respectively, suggesting that HCSC possesses more defect sites or higher density of dopants than HCSC does. These structural differences could also be what account for the observed differences in the electrochemical catalytic properties between the two materials that are described below.

It is needless to say that searching for sustainable and efficient catalysts for ORR and HOR is of high interest. This is because efficient ORR is required to produce high current densities and cell voltages in fuel cells,[36,37] and hydrazine is a highly desirable compound as fuel for fuel cells due to its higher power density, high density of hydrogen and no CO_2 emission.[12] It is with these goals in mind then that we have explored the electrocatalytic activity of the materials synthesized above for ORR and HOR (Figure 4).

The electrochemical ORR activity of HCSC and YCWC was evaluated first by acquiring cyclic voltammograms (CVs) for each material in N_2- and O_2-saturated 0.1 M KOH solutions at a scan rate of 100 mV/s. Although both materials give CVs with no peaks in the first condition (Figure S6a, Supporting Information), they both give CVs with redox peaks indicating oxygen reduction (Figure S6b, Supporting Information). The catalytic activity of HCSC and YCWC toward ORR was further evaluated by linear sweep voltammetry (LSV) on a rotating ring-disk electrode (RDE) that was running at speeds ranging from 400 to 2000 rpm in an O_2-saturated 0.1 M KOH solution at a scan rate of 10 mV/s. At 1600 rpm (Figure 4a), HCSC shows a more positive onset potential (−0.11 V vs SCE) compared with YCWC (−0.15 V vs SCE). This indicates that HCSC is a better electrocatalyst for ORR than YCWC is. This finding is further confirmed by LSV curves obtained over the materials placed on RDE that is rotating at different speeds (Figure 5). The LSV results were further used to obtain Koutechy–Levich (K–L) plots, which were found to be linear indicating that the ORR over these materials is first order.[38] Based on the slopes on K-L plots, the electron transfer number (n) per O_2 molecule in ORR over HCSC and YCWC is calculated and found to be somewhere between 3 and 4 (Figure S7a, Supporting Information). In addition, rotating ring currents were used to calculate n, along with the percentage of peroxide (H_2O_2) in the products. The results (Figure S7b and S7c, Supporting Information) indicate that the ORR proceeds through both 2- and 4-electron processes over both materials, with some differences though. The HCSC equally favors the 2-and 4-electron processes since it can generate about 50% H_2O_2 over a wide potential range. However, YCWC increasingly favors a 2-electron process more than a 4-electron process when the applied potential increases to a less negative value. Additionally, the kinetic current density is found to be higher over HCSC than over YCWC in a wide potential range (Figure 4b). HCSC also gives a slightly lower Tafel slope (96 mV/dec) compared with YCWC (98 mV/dec) (Figure S8, Supporting Information). All these results confirm that HCSC is a better electrocatalyst for ORR than YCWC, although HCSC's activity toward ORR is lower than that of the Pt/C (20 wt %) (Figure S9, Supporting Information).

The electrocatalytic properties of the materials toward hydrazine oxidation reaction (HOR) were also evaluated. The CVs obtained at a scan rate of 10 mV/s for various concentrations of hydrazine (from 0 to 64 mM) in pH = 7.4 phosphate buffer saline (PBS) are shown in Figure S10a (Supporting Information). The CVs over HCSC for hydrazine concentration of 6.4 mM show peaks starting at −0.4 V vs SCE corresponding to oxidative processes. As the concentration of hydrazine is increased, the oxidation peak current increased linearly (Figure S10b, Supporting Information). HCSC showed higher current for hydrazine oxidation during the potential of

DOI: 10.1021/am507787t
ACS Appl. Mater. Interfaces 2015, 7, 1978–1986

−0.4 to −0.1 V vs SCE (Figure 4c). Significant current associated with oxidative process is also observed over YCWC, but at less negative potential than that over HCSC; in fact, no oxidation current is observed for YCWC until the potential reaches −0.3 V vs SCE (Figure S10c, Supporting Information).

The stability of the materials in the electrocatalytic reaction is investigated by chronoamperometric measurement. The $i-t$ curves (Figure 4d) over HCSC and YCWC at a working potential of −0.15 V vs SCE in the presence of 50 mM hydrazine clearly reveal that former retains higher residual current than the latter, indicating that it is a better electrocatalyst than YCWC. The retention peak current density remains stable for HCSC during 500 cycles of CV measurements, further confirming its long-term stability (Figure S11, Supporting Information). So, overall, these results indicate that HCSC is a better electrocatalyst than YCWC for HOR too.

CONCLUSION

We have described the synthesis of heteroatom-doped carbon microparticles, denoted HCSC and YCWC, using yeast cells and yeast cell wall particles, respectively, as precursor. We have also demonstrated that the materials have the ability to electrocatalyze the ORR and the HOR. Furthermore, our results have indicated that HCSC is a more effective electrocatalyst than YCWC. This finding is not surprising given the fact that the former contains more heteroatom dopants such as oxygen, phosphorus, and nitrogen, which are mainly responsible for the electrocatalytic activity exhibited by such materials toward ORR,[7,23,24,39,40] as well as HOR.[12,14,25] Besides the nonmetallic heteroatom dopant elements, the Fe atoms present in the carbon materials we synthesized could be expected to have taken some part in the electrocatalysis, based on previous reports.[41−43] Although the mechanisms by which HCSC and YCWC electrocatalyze the reaction is not completely understood, based on the results we discussed above some insights into the structure and comparative structure-related electrocatalytic properties of the materials have been gained. Specifically, despite HCSC contains slightly lower total amount of Fe (0.048%) than YCWC (0.11%), the HCSC holds most of the Fe atoms on its surfaces while the YCWC does in its internal part. This result, combined with the fact that HCSC possesses more nonmetallic dopant elements than YCWC does, can lead to the conclusion that the biomacromolecules in the inner parts of the intact yeast cells must be indirectly responsible and account for the higher electrocatalytic activity exhibited by HCSC. In other words, the biomacromolecules (DNA, RNA, proteins) present inside the yeast cells are indirectly responsible for the higher density of such dopants in HCSC, including the relatively higher density of Fe atoms on its surfaces, and thereby its higher electrocatalytic activity.

As there are millions of microorganisms in nature, which have different morphology and compositions but can equally generate various types of carbon materials under the procedure we developed here, the method we have demonstrated here for yeast cells can serve as generic and sustainable route for making a broad range of bioderived carbons with electrocatalytic activity. Moreover, despite the electrocatalytic efficiency of the material is a bit lower than that of commercial Pt/C electrocatalysts, there is still a lot of room for improvement of the electrocatalytic activities of these materials. In particular, by coupling the method with genetic engineering, which allow generation of mutated microorganisms by insertion of unnatural amino acids into the raw materials, this proof-of-concept study could be expanded to produce various other novel carbon materials with controlled dopant density and interesting and tunable properties for electrocatalysis as well as a broad range of other applications.

ASSOCIATED CONTENT

Supporting Information

Materials characterization results, including microscopy images, N_2 adsorption/desorption, X-ray photoelectron spectra, as well as the electocatalytic evaluation results. This material is available free of charge via the Internet at http://pubs.acs.org.

AUTHOR INFORMATION

Corresponding Author

*T. Asefa. E-mail: tasefa@rci.rutgers.edu.

Notes

The authors declare no competing financial interest.

ACKNOWLEDGMENTS

T.A. acknowledges the financial support of National Science Foundation (NSF DMR-0968937 and NSF NanoEHS-1134289).

REFERENCES

(1) Ma, T.-Y.; Liu, L.; Yuan, Z. Direct Synthesis of Ordered Mesoporous Carbons. *Chem. Soc. Rev.* **2013**, *42*, 3977−4003.
(2) Shen, W.; Fan, W. Nitrogen-Containing Porous Carbons: Synthesis and Application. *J. Mater. Chem. A* **2013**, *1*, 999−1013.
(3) Zou, X.; Huang, X.; Goswami, A.; Silva, R.; Sathe, B. R.; Mikmeková, E.; Asefa, T. Cobalt-Embeeded Nitrogen-Rich Carbon Nanotubes Efficiently Catalyze Hydrogen Evolution Reaction at All pH Values. *Angew. Chem., Int. Ed.* **2014**, *126*, 4461−4465.
(4) Ma, T.-Y.; Dai, S.; Jaroniec, M.; Qiao, S.-Z. Graphitic Carbon Nitride Nanosheet-Carbon Nanotube Three-Dimensional Porous Composites as High-Performance Oxygen Evolution Electrocatalysts. *Angew. Chem., Int. Ed.* **2014**, *53*, 7281−7285.
(5) Li, M.; Zhang, L.; Xu, Q.; Niu, J.; Xia, Z. N-Doped Graphene as Catalysts for Oxygen Reduction and Oxygen Evolution Reactions: Theoretical Considerations. *J. Catal.* **2014**, *314*, 66−72.
(6) Waki, K.; Wong, R. A.; Oktaviano, H. S.; Fujio, T.; Nagai, T.; Kimoto, K.; Yamada, K. Non-Nitrogen Doped and Non-Metal Oxygen Reduction Electrocatalysts Based on Carbon Nanotubes: Mechanism and Origin of ORR Activity. *Energy Environ. Sci.* **2014**, *7*, 1950−1958.
(7) Yang, D. S.; Bhattacharjya, D.; Inamdar, S.; Park, J.; Yu, J. S. Phosphorus-Doped Ordered Mesoporous Carbons with Different Lengths as Efficient Metal-Free Electrocatalysts for Oxygen Reduction Reaction in Alkaline Media. *J. Am. Chem. Soc.* **2012**, *134*, 16127−16130.
(8) Yang, D.-S.; Chaudhari, S.; Rajesh, K. P.; Yu, J.-S. Preparation of Nitrogen-Doped Porous Carbon Nanofibers and the Effect of Porosity, Electrical Conductivity, and Nitrogen Content on Their Oxygen Reduction Performance. *ChemCatChem.* **2014**, *6*, 1236−1244.
(9) Zhao, A.; Masa, J.; Schuhmann, W.; Xia, W. Activation and Stabilization of Nitrogen-Doped Carbon Nanotubes as Electrocatalysts in the Oxygen Reduction at Strongly Alkaline Conditions. *J. Phys. Chem. C* **2013**, *117*, 24283−24291.
(10) Lee, J.-S.; Jo, K.; Lee, T.; Yun, T.; Cho, J.; Kim, B.-S. Facile Synthesis of Hybrid Graphene and Carbon Nanotubes as a Metal-Free Electrocatalyst with Active Dual Interfaces for Efficient Oxygen Reduction Reaction. *J. Mater. Chem. A* **2013**, *1*, 9603−9607.
(11) Silva, R.; Voiry, D.; Chhowalla, M.; Asefa, T. Efficient Metal-Free Electrocatalysts for Oxygen Reduction: Polyaniline-Derived N- and O- Doped Mesoporous Carbons. *J. Am. Chem. Soc.* **2013**, *135*, 7823−7826.

DOI: 10.1021/am507787t
ACS Appl. Mater. Interfaces 2015, 7, 1978−1986

(12) Meng, Y.; Zou, X.; Huang, X.; Goswami, A.; Liu, Z.; Asefa, T. Polypyrrole-Derived Nitrogen and Oxygen Co-Doped Mesoporous Carbons as Efficient Metal-Free Electrocatalysts for Hydrazine Oxidation. *Adv. Mater.* **2014**, *26*, 6510−6516.
(13) Meng, Y.; Voiry, D.; Goswami, A.; Zou, X.; Huang, X.; Chhowalla, M.; Liu, Z.; Asefa, T. N-, O-, and S-Tridoped Nanoporous Carbons as Selective Catalysts for Oxygen Reduction and Alcohol Oxidation Reactions. *J. Am. Chem. Soc.* **2014**, *136*, 13554−13557.
(14) Silva, R.; Al-Sharab, J.; Asefa, T. Edge-Plane-Rich Nitrogen-Doped Carbon Nanoneedles and Efficient Metal-Free Electrocatalysts. *Angew. Chem., Int. Ed.* **2012**, *51*, 7171−7175.
(15) Liang, Y.; Wu, D.; Fu, R. Carbon Microfibers with Hierarchical Porous Structure From Electrospun Fiber-like Natural Biopolymer. *Sci. Rep.* **2013**, *3*, 1119.
(16) Park, M.; Ryu, J.; Kim, Y.; Cho, J. Corn Protein-Derived Nitrogen-Doped Carbon Materials with Oxygen-Rich Functional Groups: A Highly Efficient Electrocatalyst for All-Vanadium Redox Flow Batteries. *Energy Environ. Sci.* **2014**, *7*, 3727−3735.
(17) Maruyama, J.; Abe, I. Carbonized Hemoglobin Functioning as a Cathode Catalyst for Polymer Electrolyte Fuel Cells. *Chem. Mater.* **2006**, *18*, 1303−1311.
(18) Chaudhari, N. K.; Song, M. Y.; Yu, J. S. Heteroatom-Doped Highly Porous Carbon From Human Urine. *Sci. Rep.* **2014**, *4*, 5221.
(19) Xia, Y.; Xiao, Z.; Dou, X.; Huang, H.; Lu, X.; Yan, R.; Gan, Y.; Zhu, W.; Tu, J.; Zhang, W.; Tao, X. Green and Facile Fabrication of Hollow Porous MnO/C Microspheres from Microalgaes for Lithium-Ion Batteries. *ACS Nano* **2013**, *7*, 7083−7092.
(20) Zhang, H.; Wang, Y.; Wang, D.; Li, Y.; Liu, X.; Liu, P.; Yang, H.; An, T.; Tang, Z.; Zhao, H. Hydrothermal Transformation of Dried Grass into Graphitic Carbon-based High Performance Electrocatalyst for Oxygen Reduction Reaction. *Small* **2014**, *10*, 3371−3378.
(21) Chen, P.; Wang, L.-K.; Wang, G.; Gao, M.-R.; Ge, J.; Yuan, W.-J.; Shen, Y.-H.; Xie, A.-J.; Yu, S.-H. Nitrogen-Doped Nanoporous Carbon Nanosheets Derived from Plant Biomass: An Efficient Catalyst for Oxygen Reduction Reaction. *Energy Environ. Sci.* **2014**, *7*, 4095−4103.
(22) Ding, J.; Wang, H.; Li, Z.; Kohandehghan, A.; Cui, K.; Xu, Z.; Zahiri, B.; Tan, X.; Lotfabad, E. M.; Olsen, B. C.; Mitlin, D. Carbon Nanosheet Frameworks Derived from Peat Moss as High Performance Sodium Ion Battery Anodes. *ACS Nano* **2013**, *7*, 11004−11015.
(23) Jiao, Y.; Zheng, Y.; Jaroniec, M.; Qiao, S. Z. Origin of the Electrocatalytic Oxygen Reduction Activity of Graphene-based Catalysts: A Roadmap to Achieve the Best Performance. *J. Am. Chem. Soc.* **2014**, *136*, 4394−4403.
(24) Cheon, J. Y.; Kim, J. H.; Kim, J. H.; Goddeti, K. C.; Park, J. Y. Intrinsic Relationship between Enhanced Oxygen Reduction Reaction Activity and Nanoscale Work Function of Doped Carbons. *J. Am. Chem. Soc.* **2014**, *136*, 8875−8878.
(25) Yu, D.; Wei, L.; Jiang, W.; Wang, H.; Sun, B.; Zhang, Q.; Goh, K.; Si, R.; Chen, Y. Nitrogen Doped Holey Graphene as an Efficient Metal-Free Multifunctional Electrochemical Catalyst for Hydrazine Oxidation and Oxygen Reduction. *Nanoscale* **2013**, *5*, 3457−3464.
(26) Liu, W.; Brock, A.; Chen, S.; Chen, S.; Schultz, P. G. Genetic Incorporation of Unnatural Amino Acids into Proteins in Mammalian Cells. *Nat. Methods* **2007**, *4*, 239−244.
(27) Osumi, M. The Ultrastructure of Yeast: Cell Wall Structure and Formation. *Micron* **1998**, *29*, 207−233.
(28) Weinzierl, D.; Lind, A.; Kunz, W. Hollow SiO_2 Microsphers Produced by Coating Yeast Cells. *Cryst. Growth Des.* **2009**, *9*, 2318−2323.
(29) Liu, S.; Bian, W.; Yang, Z.; Tian, J.; Jin, C.; Shen, M.; Zhou, Z.; Yang, R. A Facile Synthesis of $CoFe_2O_4$/Biocarbon Nanocomposites as Efficient Bi-Functional Electrocatalysts for the Oxygen Reduction and Oxygen Evolution Reaction. *J. Mater. Chem. A* **2014**, *2*, 18012−18017.
(30) Soto, E. R.; Ostroff, G. R. Characterization of Multilayered Nanoparticles Encapsulated in Yeast Cell Wall Particles for DNA Delivery. *Bioconjugate Chem.* **2008**, *19*, 840−848.
(31) Maldonado-Hódar, F. J.; Moreno-Castilla, C.; Rivera-Utrilla, J.; Hanzawa, Y.; Yamada, Y. Catalytic Graphitization of Carbon Aerogels by Transition Metals. *Langmuir* **2000**, *16*, 4367−4373.
(32) Fakhrullin, R. F.; Zamaleeva, A. I.; Minullina, R. T.; Konnova, S. A.; Paunov, V. N. Cyborg Cells: Functionalisation of Living Cells with Polymers and Nanomaterials. *Chem. Soc. Rev.* **2012**, *41*, 4189−4206.
(33) Zamaleeva, A. I.; Sharipova, I. R.; Porfireva, A. V.; Evtugyn, G. A.; Fakhrullin, R. F. Polyelectrolyte-Mediated Assembly of Multiwalled Carbon Nanotubes on Living Yeast Cells. *Langmuir* **2010**, *26*, 2671−2679.
(34) Yang, S. H.; Ko, E. H.; Jung, Y. H.; Choi, I. S. Bioinspired Functionalization of Silica-Encapsulated Yeast Cells. *Angew. Chem., Int. Ed.* **2011**, *50*, 6115−6118.
(35) Konnova, S. A.; Sharipova, I. R.; Demina, T. A.; Osin, Y. N.; Yarullina, D. R.; Ilinskaya, O. N.; Lvov, Y. M.; Fakhrullin, R. F. Biomimetic Cell-Mediated Three-Dimensional Assembly of Halloysite Nanotubes. *Chem. Commun.* **2013**, *49*, 4208.
(36) Winter, M.; Brodd, R. J. What Are Batteries, Fuel Cells, and Supercapacitors? *Chem. Rev.* **2004**, *104*, 4245−4269.
(37) Gewirth, A. A.; Thorum, M. S. Electroreduction of Dioxygen for Fuel-Cell Applications: Materials and Challenges. *Inorg. Chem.* **2010**, *49*, 3557−3566.
(38) Liang, Y.; Li, Y.; Wang, H.; Zhou, J.; Wang, J.; Regier, T.; Dai, H. Co_3O_4 Nanocrystals on Graphene as a Synergistic Catalyst for Oxygen Reduction reaction. *Nat. Mater.* **2011**, *10*, 780−786.
(39) Rao, C. V.; Cabrera, C. R.; Ishikawa, Y. In Search of the Active Site in Nitrogen-Doped Carbon Nanotube Electrodes for the Oxygen Reduction Reaction. *J. Phys. Chem. Lett.* **2010**, *1*, 2622−2627.
(40) Oh, H. S.; Oh, J. G.; Roh, B.; Hwang, I.; Kim, H. Development of Highly Active and Stable Non-Precious Oxygen Reduction Catalysts for PEM Fuel Cells Using Polypyrrole and a Chelating Agent. *Electrochem. Commun.* **2011**, *13*, 879−881.
(41) Liang, H. W.; Wei, W.; Wu, Z. S.; Feng, X.; Mullen, K. Mesoporous Metal-Nitrogen-Doped Carbon Electrocatalysts for Highly Efficient Oxygen Reduction Reaction. *J. Am. Chem. Soc.* **2013**, *135*, 16006−16005.
(42) Guo, Z.; Jiang, C.; Teng, C.; Ren, G.; Zhu, Y.; Jiang, L. Sulfur, Trace Nitrogen and Iron Codoped Hierarchically Porous Carbon Foams as Synergistic Catalysts for Oxygen Reduction Reaction. *ACS Appl. Mater. Interfaces* **2014**, *6*, 21454−21460.
(43) Liu, J.; Sun, X.; Song, P.; Zhang, Y.; Xing, W.; Xu, W. High-Performance Oxygen Reduction Electrocatalysts Based on Cheap Carbon Black, Nitrogen, and Trace Iron. *Adv. Mater.* **2013**, *25*, 6879−6883.

DOI: 10.1021/am507787t
ACS Appl. Mater. Interfaces 2015, 7, 1978−1986